Pergamon

Int. J. Heat Mass Transfer. Vol. 38, No. 13, pp. 2445–2456, 1995

0017-9310/95 $9.50+0.00

0017-9310(94)00371-8

Mixed convection flow and heat transfer in a heated vertical convergent channel

T. M. HUANG, C. GAU and WIN AUNG†

Institute of Aeronautics and Astronautics, National Cheng Kung University, Taiwan, Republic of China

(*Received* 3 *February* 1994 *and in final form* 20 *November* 1994)

Abstract—Experimental studies of the mixed convection flow and heat transfer in a vertical convergent channel have been carried out. One of the side walls which maintains the vertical position is heated uniformly, and the opposite wall which has a convergence angle of 3° is insulated. The ratio of the height to the width at the inlet of the channel is 15. During the experiments, the Reynolds number ranges from 100 to 4000 and the buoyancy parameter, Gr/Re^2, ranges from 0.3 to 907. Flow structure inside the channel is visualized with a heated smoke wire. For both assisted and opposed convection, flow reversal occurs only in the upstream of the channel but not in the downstream where rapid acceleration of flow occurs and the transport process is dominated by forced convection. For assisted convection, the reversed flow forms a steady recirculation cell along the insulated wall, and has no effect on the heat transfer. For opposed convection, the reversed flow occurs along the heated wall, and is unstable and sometimes generates a number of vortices and becomes turbulent. This flow can significantly enhance the heat transfer along the heated wall. Temperature fluctuations at different locations are measured and used to indicate oscillations and fluctuations of the reversed flow. The effect of the buoyancy parameter on the reversed flow structure and the Nusselt number is presented and discussed. The Nusselt number results are correlated in terms of relevant nondimensional parameters for both pure forced and mixed convection, respectively. For the purpose of comparison, the Nusselt numbers for parallel-plate channel are also measured and presented.

INTRODUCTION

The combined free and forced convection in a symmetrically or asymmetrically heated vertical passage has received considerable attention for its practical application in solar energy collectors, heat exchangers, geothermal energy systems, and the cooling process of nuclear reactors and modern electronic equipment. In modern electronic devices, particularly, circuit density as well as power dissipation of electronic components have become very large due to advances of current technology, which may result in overheat of the system. Therefore, large amount of heat must be carried away by a suitable method in order to maintain reliable performance and long life of system.

Electronic components are usually mounted on arrays of vertical circuit boards which form parallel-plate passages through which the coolant circulates. Depending on the cooling scheme, the power density or the overall heat dissipation of the circuit boards, the coolant may be driven by free, mixed or pure forced convection. As the power density becomes large, buoyancy force may be generated in the flow which can distort both the velocity and the temperature profiles. To some extent, flow reversal may occur in the channel, which can significantly affect the stability and the structure of the flow, the wall friction and the heat transfer along the wall. Under certain circumstances the circuit boards may be slightly tilted, and turn the passages into a convergent or a divergent channel. The convergence of the channel can accelerate the upward flowing mainstream while the divergence can decelerate the flow. It is expected that both convergence and the divergence of the channel can have a significant effect on the occurrence and the structure of the reversed flow, and can change the heat transfer characteristics inside the channel.

Unfortunately, to the best knowledge of the authors, relevant studies of mixed convection in a heated vertical convergent (that is, smaller opening at the exit) or divergent (smaller opening at the entrance) channel are non-existent. The prior studies on the flow and heat transfer in a convergent or a divergent channel are mostly concerned with pure forced convection. By assuming that the family of straight lines passing through the source or sink constitute the streamlines of the flow, the governing equations of the system can be greatly simplified and their solution has been obtained [1]. This type of flow is called Jeffery–Hamel flow. The thermal problem of Jeffery–Hamel flow with constant wall temperature or a variation in wall heat flux, $q_w \sim 1/r$, where r denotes the axial distance from the source or the sink of the flow, has been studied by several investigators [2–5]. By neglecting the axial diffusion term in the energy equation and applying the method of superposition, Shiina [5] obtains a general solution for boundary condition of

† Permanent address: National Science Foundation, Arlington, VA 22230, U.S.A.

NOMENCLATURE

A	cross section area of channel	T	temperature
b	channel gap at the inlet of the channel	u_0	inlet velocity
D_h	hydraulic diameter of the channel, $2b$	x, y	coordinate parallel, and normal to the heated wall.
g	gravitational acceleration		
Gr	Grashof number, $g\beta q D_h^4/kv^2$		
h	convective heat transfer coefficient		
$\bar{h}$	average heat transfer coefficient	Greek symbols	
k	thermal conductivity of air	β	coefficient of expansion
Nu	local Nusselt number, hD_h/k	v	kinematic viscosity.
$\overline{Nu}$	average Nusselt number, $\bar{h}D_h/k$		
Pr	Prandtl number, v/α		
q	heat flux	Subscript	
Re	Reynolds number defined at the inlet of the channel, $u_0 D_h/v$	b	refers to bulk mean
		0	refers to inlet.

the kind $q_w \sim r^m$. Dey and Nath [6] use the boundary layer approximation to find the temperature distributions of the thermal boundary layer in a convergent channel with axial variation in wall heat flux. However, due to the assumption of straight streamline contours, practical application of this type of flow is very limited, especially for a divergent channel where separation of flow occurs.

For developing flow in a convergent channel, a limited number of studies have been performed [7, 8] for pure forced convection and the results indicate that the velocity profile is more likely to be 'fully developed' for small angles of convergence; further, the Nusselt number increases with the convergence angle. Su and Lin [9, 10] obtained numerical results for both convergent and divergent ducts and concluded that both the pressure drop and the Nusselt number increased with the convergent or the divergent angle. Experimental work is also found for turbulent flow in a divergent channel with fully developed inlet velocity [11, 12]. Both the velocity and the pressure drop across the convergent section have been measured. The velocity profile in the inner layer near the wall is found to be independent of the pressure gradient in the mainstream, while that in the outer layer can be represented by the velocity profile of a jet [11].

Relevant work in a convergent or a divergent channel is the natural convection experiments performed by Sparrow *et al.* [13, 14] who have considered symmetrical, constant wall temperature conditions. The experimental results are compared with the numerical predictions under the same condition in a convergent channel, and the agreement is found to be very good. In addition, correlations for the parallel-plate, the convergent, and the divergent channel have been made by these authors. Flow recirculation is found in the center portion of the divergent channel, which does not play an important role in the heat transfer. Since the heat transfer coefficient h in their report is defined as $h = Q/A(T_w - T_\infty)$, as in type for boundary layer flow, it appears that the flow recirculation outside the boundary layer does not significantly affect the heat transfer inside when turbulence is absent.

A review of mixed convection in a vertical channel indicates an overwhelming number of references. However, almost all the work completed thus far is dedicated to that on parallel-walled passages such as vertical or inclined tubes [15, 16], annuli [17, 18] and parallel-plate ducts [19, 20]. Data on parallel-walled passages give some insight to the current problem. A comprehensive review of mixed convection in a vertical pipe or channel has been thoroughly presented by Aung [21] and Jackson *et al.* [22]. In the parallel plate channel, Wirtz *et al.* [23, 24] have recently performed a LDV measurement and holographic visualization for opposed convection. The average Nusselt number over the entire heated plate can increase slightly when the wall heat flux is high [23]. The increase in the Nusselt number is attributed to the destabilization of viscous flow adjacent to the heated wall by the opposing buoyancy which can cause a high degree of turbulence intensity at the exit. Baek *et al.* [25] have presented a numerical analysis and experimental measurements of velocity profile for assisted convection in a channel with asymmetrical wall temperatures. At low Grashof number, the velocity profile predicted agrees well with the experiments, while at high Grashof number the velocity distortion predicted underestimates in the middle region and overestimates in the downstream region of the channel. The deviation between the data and the prediction is attributed to the transition to turbulent flow which is found experimentally at high Grashof number. Although heat transfer results are not presented in their report, significant enhancement in heat transfer can be expected. Gau *et al.* [26, 27] have experimentally studied the reversed flow structure and heat transfer in a finite asymmetrically heated parallel-plate channel. Flow reversal can occur at relatively low buoyancy parameter, Gr/Re^2, for opposed convection and at large Gr/Re^2 for assisted convection. The oscillation of flow induced by the reversed flow is visualized. The

Nusselt numbers based on the inlet temperature of the flow for both assisted and opposed convection are measured. A penetration model of the reversed flow is developed, and the prediction agrees with the data for small Reynolds number and large buoyancy parameter. However, the results in the parallel-plate channel cannot be used to predict the complicated mixed convection flow and heat transfer in a convergent or a divergent channel. A systematic study of mixed convection in these channels is needed.

The present paper describes an experimental study of mixed convection in a heated vertical convergent channel. A uniform air flow enters the channel, and exits to the ambient after passing the test section. One of the channel walls which is maintained in the vertical position is heated uniformly, while the opposite wall which has a convergence angle of 3°, with one end tilted toward the opposed wall, is well-insulated. The objective of this work is to study the mixed convection flow, especially the reversed flow structure and the heat transfer, in a heated vertical convergent channel. Results of both the flow visualization using smoke wire and the heat transfer measurements along the heated wall are presented. The effects of the buoyancy parameter and the Reynolds number on the flow structure and the Nusselt number are reported. For the purpose of comparison, the heat transfer coefficient in the parallel-plate channel is also measured and presented.

EXPERIMENTAL APPARATUS AND PROCEDURES

Experiments are performed in a plexiglas channel. The channel is 45 cm in length, 20 cm in width inside and 3 cm in gap at the entrance. One of the vertical walls can be tilted, in the current experiment, with a 3° convergent angle. The angle of the inclined wall can be adjusted as desired. For parallel plate channel, however, the inclined wall is adjusted to be parallel to the opposite wall. This opposite side wall is made of 2 cm thick balsa wood and electrically heated. This is achieved by gluing a number of 0.015 cm thick stainless steel foil strips on the entire wall and passing electric current through the foil heater. DC power is used to provide the electric energy for generating the desired heat flux. The heat flux can be determined by the electric voltage and current passing through the foil. The electric voltage drop due to the contact resistance between the heating strips and the terminals, which connect the heating strips with the DC power supply, has been taken into account. This kind of voltage drop is also noticed in the experiment by Webb *et al.* [28]. For better insulation, a 12 cm thick foamed rubber is glued on the back of the heated wall. In addition, all the other side walls are wrapped with 3 cm thick foamed rubber.

The heated wall is instrumented with 89 chromel–alumel thermocouples epoxied on the back at 5-mm intervals along the centerline of the wall. Eleven more thermocouples are positioned 5 cm away from the centerline to monitor the end wall temperature variations. It is found that the maximum spanwise variation of the wall temperatures (in Celsius) is less than 3%. This indicates that a two-dimensional transport process can be maintained when flow reversal is absent. Since the surface temperature of the opposite wall is needed for estimating the radiation loss from the heated wall, five additional thermocouples are embedded along the surface of the wall. All thermocouples are calibrated in a constant temperature bath and the measurement error is found to be within $\pm 0.1°C$. All the temperature signals are acquired with a FLUKE-2287 A data logger connected to a computer for direct processing. The temperature data are taken when the entire system reaches steady state, usually in 3–4 h.

During the flow visualization experiments, a thin, electrically heated wire coated with oil is used to generate the smoke. Fine iron powders are added into the oil, as suggested by Fukamachi *et al.* [29], to provide smoke of a better quality. The smoke wire can be inserted through different small holes in the insulated wall. A vertical sheet of light perpendicular to the insulated wall is used for illumination. The flow patterns at the upstream, the central and the downstream regions can be observed and recorded. In order to generate visualizable smoke without disturbing the entire flow, the electrical power imposed on the heated wire is carefully controlled. In addition, to minimize the possible effect of the smoke on the flow structure, smoke is generated periodically by turning off the electric current passing through the wire intermittently.

For assisted convection, air enters the channel from its larger end which is located at the bottom. For opposed convection, however, the convergent channel is turned upside down, and air enters the channel from the top. For pure forced convection experiments, the buoyancy force inside the channel should be minimized and this is accomplished by situating the channel in a horizontal position. To accommodate the above situations, the entire channel and the wind tunnel which includes the diffuser, the settling chamber and the contraction section are bolted together and placed on a rotatable frame. To study the buoyancy effect on the transport process inside the channel, the flow velocity needs to be very low. In addition, due to the occurrence of flow reversal, the entire flow may become unsteady and significantly affected by the noise and turbulence generated by the blower. Therefore, a very large noise reduction chamber is constructed that has multiple passages and layers of sponge glued to the inside. Since a pitot tube cannot accurately measure the slow velocity of interest here, the velocity in the channel is measured with a TSI hot wire anemometer. To obtain increased accuracy, an improved calibration system, which was originally designed by Chen and Miau [30], is used. During the calibration process, the hot wire is placed on a

transverse mechanism that is enclosed in a quiescent room. The transverse velocity of the probe, which corresponds to the velocity of the air flow passing through the wire, is controlled by a step motor of variable speed. By this means, a calibration curve for the air flow velocity through the wire and the corresponding compensation voltage across the wire can be obtained. The entire velocity profile at the inlet to the channel is measured and found to be very flat at both high and very low entrance velocity conditions. The turbulence intensity measured at the entrance of the channel is 2.1% for entrance velocity at 0.27 m s^{-1} and 0.7% for entrance velocity at 1.59 m s^{-1}.

The total heat input in a single heating strip can be determined by the electric voltage and current passing through the strip. However, both the conduction and the radiation losses from each heating strip need to be accounted for and substracted from the total energy supplied by the heater. Therefore, the local heat transfer coefficient is evaluated by the following equation:

$$h_r = (q_t - q_{rad} - q_{cond})/(T_w - T_r) \quad (1)$$

where r refers to the bulk mean condition or the inlet condition. The conduction loss from the heated wall is estimated by a one-dimensional conduction equation in a composite wall. The procedure to calculate the radiation loss from the heated wall is very similar to the one described in [28] and will not be repeated here. The thermophysical properties in the local Nusselt number are evaluated at the bulk mean temperature of the flow, while those in the Reynolds and Grashof numbers are evaluated at the inlet.

Since the channel flow exits directly to the ambient, the heat loss is relatively large near the exit. Therefore, the last three heating strips are used only as guard heaters. Relatively large heat loss in the exit region is also found in the experiments by Wirtz and Mckinley [23] and Webb and Hill [28]. To avoid the circulation of ambient flow which may affect the exit condition of the channel, a wind shield is made and put outside the channel near the exit region. The uncertainty of the experimental data is determined according to the procedure proposed by Kline and McClintock [31]. The maximum uncertainty of local Nusselt number is 5.6%, while the Reynolds and Grashof number are 6.2 and 7.8%, respectively.

RESULTS AND DISCUSSIONS

Flow visualizations

The reversed flow patterns for buoyancy-assisted and opposed convection in the parallel-plate channel have been illustrated and discussed by Gau *et al.* [26, 27], and will be compared with those for the convergent channel in the following discussion. For assisted convection in a convergent channel, no flow reversal is found when the buoyancy parameter is small. When Gr/Re^2 is large enough ($Gr/Re^2 > 100$), a recirculation bubble occurs near the insulated wall, as shown in Fig. 1, where the heated wall is on the left and the insulated wall on the right. It appears that the reversed flow structure occurring in the convergent channel is somewhat different from the one in the parallel-plate channel. For parallel-plate channel, flow reversal is triggered when buoyancy force becomes so large in the downstream of the channel that natural convection starts to dominate the transport process. In this event, the total mass flow rate furnished by the blower is less than the total mass flow rate driven by the buoyant heated flow along the heated vertical plate. Therefore, a minimum pressure is created inside the channel and cold air is sucked into the channel along the insulated wall from outside, forming a V-shaped circulation flow. For a convergent channel, however, a minimum pressure can also be created that sucks the air to move upstream along the insulated wall from the downstream region. Therefore, a steady recirculation cell can be formed as shown in Fig. 1(a). In the downstream region and near the exit of the convergent channel, no flow reversal is found, as shown in Fig. 1(b). This is due to the fact that the convergence of the channel makes the flow in the downstream region move faster so that the transport process there is dominated by forced convection. Despite the fact that the exact location for the top of the recirculation cell could not be clearly identified, the size of the recirculation flow is found to increase with increasing Gr/Re^2. With the recirculation flow, the entire flow is still very steady, no oscillation or transition to turbulent flow occurs within the range of Gr/Re^2 covered.

For opposed convection, flow reversal can also occur in the convergent channel when the buoyancy parameter is large enough. For the case with $Gr/Re^2 = 10$ and $Re = 1000$, the reversed flow occurs, as shown in Fig. 2 where the right wall is heated uniformly and the left wall is insulated. This is the buoyancy parameter which is slightly higher than the threshold value for the occurrence of flow reversal. The mainstream enters the channel from the top and moves downstream (downward) while the reversed flow is initiated in the downstream along the heated wall and moves upstream (upward), as shown in Fig. 2(a). The small protrusions appearing along the heated wall are the terminals connecting the heating strips with the d.c. power supplies. The terminals are embedded in the side wall and cannot disturb the entire flow. The reversed flow initiating in the downstream region is very thin; it is heated, thickens and accelerates as it moves upstream. Due to the counterflow motion, the reversed flow becomes unstable. The interface between the reversed flow and the mainstream becomes wavy and is distorted, as shown in Fig. 2(b). This leads to the result that the highest point of the reversed flow moves up and down periodically. The highest point that the reversed flow can reach is determined by the balance between the buoyancy force inside the reversed flow and the inertia and viscous forces imposed by the mainstream. A higher heat

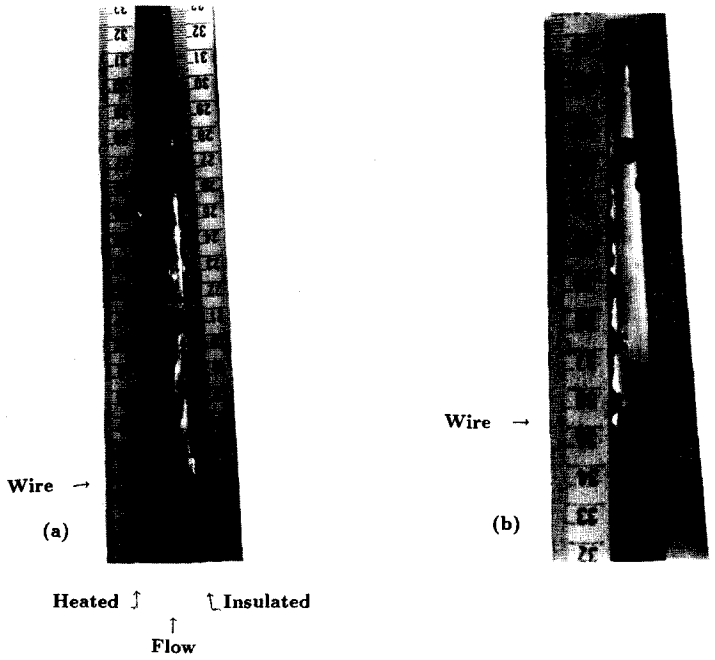

Fig. 1. Reversed flow structure for assisted convection in a convergent channel with $Gr/Re^2 = 250$ and $Re = 200$: (a) upstream region; (b) downstream region.

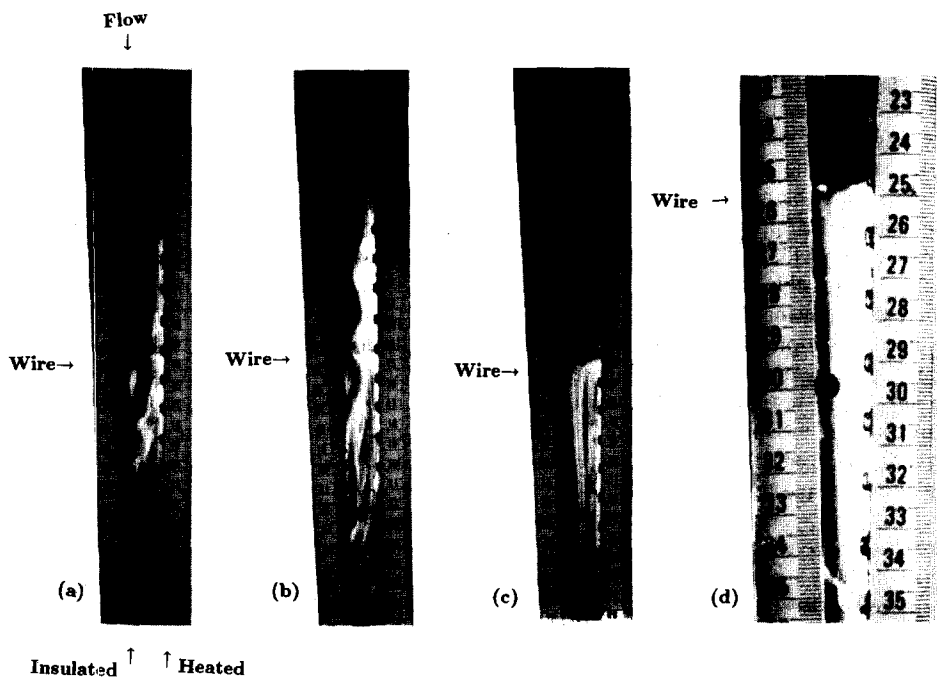

Fig. 2. Reversed flow structure for opposed convection in a convergent channel with $Gr/Re^2 = 10$ and $Re = 1000$.

flux along the wall leads to a higher buoyancy force which can move the reversed flow further upstream (that is, toward the top of the channel). However, the reversed flow may become so unstable that it can be completely 'washed' away periodically by the mainstream, as shown in Fig. 2(c). In the absence of the reversed flow, the entire flow becomes steady in this period of time (lasting approximately 8 s). After this, the reversed flow is initiated again in the downstream. The whole process is repeated, leading to oscillations of flow in the downstream.

In the far downstream region, no flow reversal is found, as shown in Fig. 2(d) in which the smoke wire is located at $x = 25$ cm. This is due to the fact that

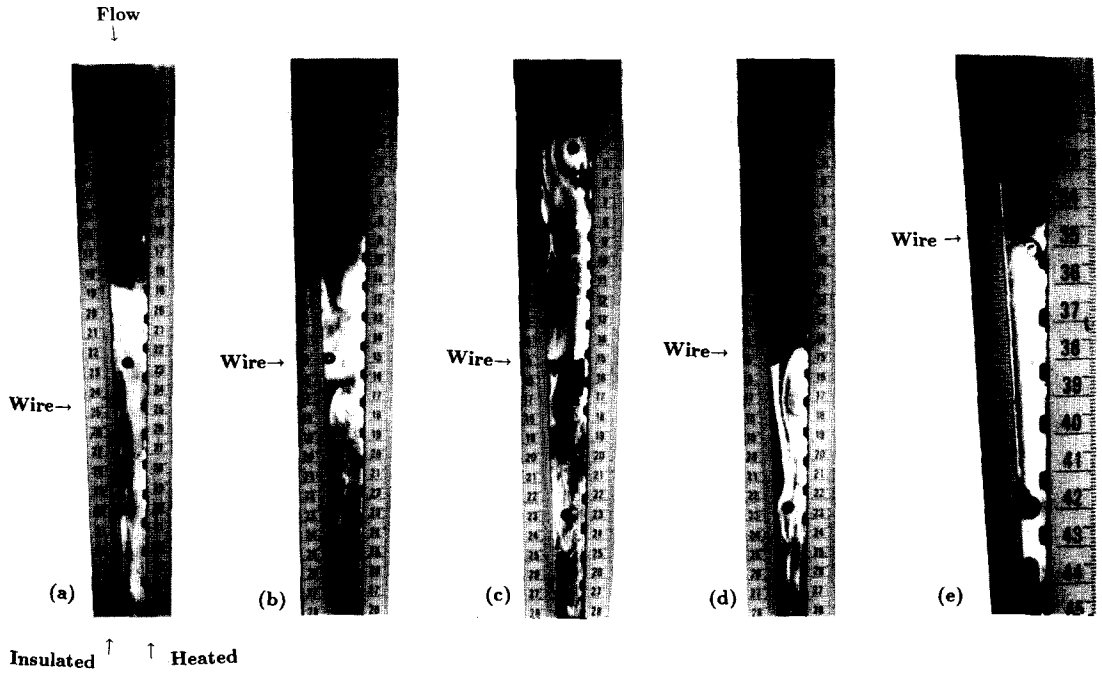

Fig. 3. Reversed flow structure for opposed convection in a convergent channel with $Gr/Re^2 = 40$ and $Re = 500$.

the buoyancy force of the reversed flow in this downstream region is relatively small and the rapid acceleration of the mainstream makes its inertia force relatively large so that it can 'wash' away the reversed flow located along the heated wall. Therefore, the reversed flow cannot be initiated near the exit of the convergent channel as opposed to the situation in the parallel-plate channel [32]; however, initiation of the reversed flow is possible somewhere in the middle region where the buoyancy force is large enough.

As the heat flux along the wall increases, i.e. as the buoyancy parameter of the system increases, the highest point of the reversed flow moves upstream with the lowest point moving downstream. Therefore, the extent that the reversed flow travels increases with increasing buoyancy parameter as shown in Fig. 3 for $Gr/Re^2 = 40$ and $Re = 500$. The reversed flow for the case where the smoke wire located at $x = 25$ cm can be observed in Fig. 3(a); the reversed flow in the downstream region is absent for $Gr/Re^2 = 10$ and $Re = 1000$. The phenomenon of repeated initiation, growth, mixing and washing away of the reversed flow is also observed and shown in Fig. 3(b), (c) and (d). However, the frequency for the repeated 'washing' away of the reversed flow is higher. The time period for the initiation of the reversed flow is approximately 3 s. The intense mixing with the mainstream makes the reversed flow three-dimensional. In the downstream near the exit the flow is very steady, and no flow reversal is found, as shown in Fig. 3(e). It appears that the acceleration of flow due to the convergence of channel is still significant near the exit, and the flow process is dominated by forced convection.

When the buoyancy parameter is very large, the reversed flow layer becomes very thick and is highly unstable. The strong mixing of the reversed flow with the mainstream can induce a number of vortices and cause a transition from laminar to turbulent flow as shown in Fig. 4(a). The reversed flow also can penetrate directly to the top of the channel and exit to the outside as shown in Fig. 4(b). The repeated initiation, growth, mixing and washing way of the reversed flow can still be observed, except that the frequency for the initiation of the reversed flow is higher. When the reversed flow is washed away, it takes less than one second to initiate a new reversed flow. Due to the high buoyancy parameter, the reversed flow and its strong interaction and mixing with the mainstream can still be observed, as shown in Fig. 4(d), with smoke wire located at $x = 35$ cm, which is closer to the exit. Despite the fact that the vortices and the turbulence generated upstream can propagate downstream, the turbulence in the downstream region is not so intense as those in the upstream. This is apparently caused by the strong acceleration of flow which suppresses the turbulence.

Temperature fluctuations

A very thin thermocouple probe having a wire diameter of 0.1 mm is inserted into the center of the channel at different locations to measure the temperature fluctuations of the flow. For assisted convection, no oscillations or fluctuations of temperatures are found in the entire channel in the range of Gr/Re^2 covered since the reversed flow which occurs is very steady and laminar. For opposed convection,

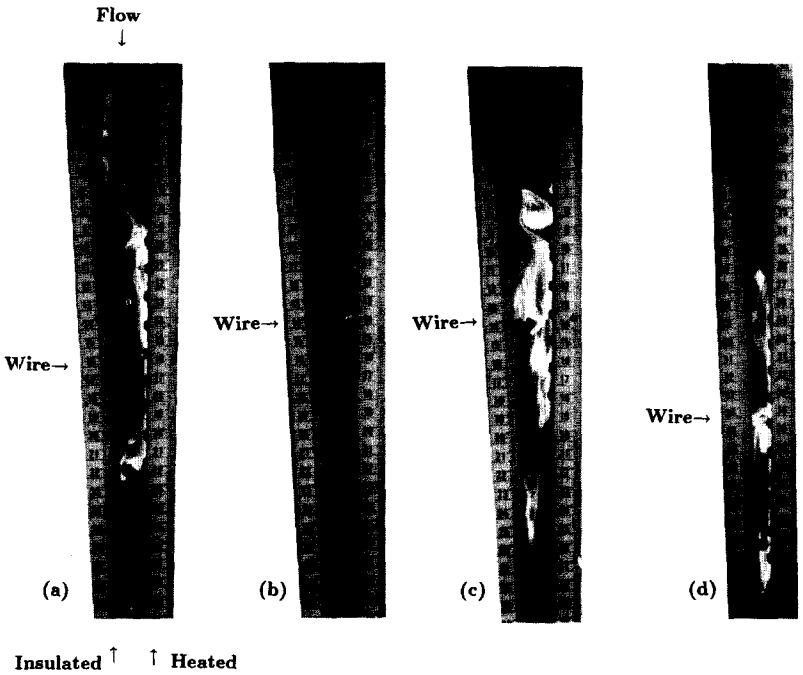

Fig. 4. Reversed flow structure for opposed convection in a convergent channel with $Gr/Re^2 = 907$ and $Re = 105$.

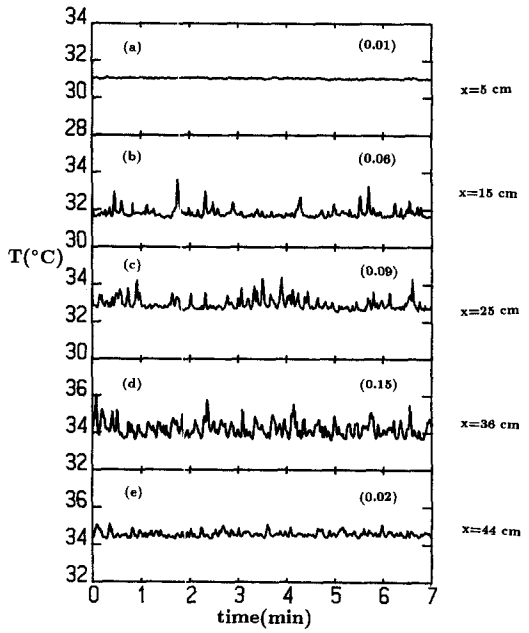

Fig. 5. Temperature fluctuations for opposed convection in a convergent channel with $Gr/Re^2 = 10$ and $Re = 1000$ at (a) $x = 5$ cm, (b) $x = 15$ cm, (c) $x = 25$ cm, (d) $x = 36$ cm and (e) $x = 44$ cm.

however, the flow becomes unstable and oscillations of temperature are found to accompany the reversed flow. Figure 5 shows the fluctuations of temperatures at different positions in the convergent channel for $Gr/Re^2 = 10$ and $Re = 1000$. The value in the parenthesis of each figure is the root-mean-square of the temperature fluctuations at each location. As mentioned previously in connection with flow visualization, the reversed flow has a slow motion of oscillation, it is the oscillation of the flow makes the fluctuations of temperature occur. As the thermocouple probe moves downstream, both the amplitude and the frequency of the temperature fluctuation increase, as shown in Fig. 5(b), due to enhanced oscillations. Upstream of the reversed flow, however, no oscillation or fluctuation of temperature is found, as shown in Fig. 5(a). It appears that the oscillation of the flow does not propagate upstream; it does propagate in the downstream region, causing relatively large fluctuations of temperature downstream, as shown in Fig. 5(c) and (d). However, the convergence of the channel can accelerate the flow which has the effect of suppressing the flow oscillations and reducing the amplitude of the temperature fluctuations. The suppression effect becomes more evident further downstream, as shown in Fig. 5(e), for $x = 44$ cm which is close to the exit. It has been found [33, 34] that the strong acceleration of flow can completely suppress the turbulence and cause a reverse transition to laminar flow. Therefore, the relaminarization of flow in the downstream area can be expected in a channel having a large angle of convergence.

When the buoyancy parameter is very large, the strong interaction and mixing between the reversed flow and the mainstream can lead to relatively large amplitude and high frequency of temperature fluctuations, as shown in Fig. 6(a) and (b). However, the amplitude of the temperature fluctuations gradually reduces, as shown in Fig. 6(c), (d) and (e), as the flow moves downstream. This is due to the suppression of turbulence by the accelerated flow. The suppression

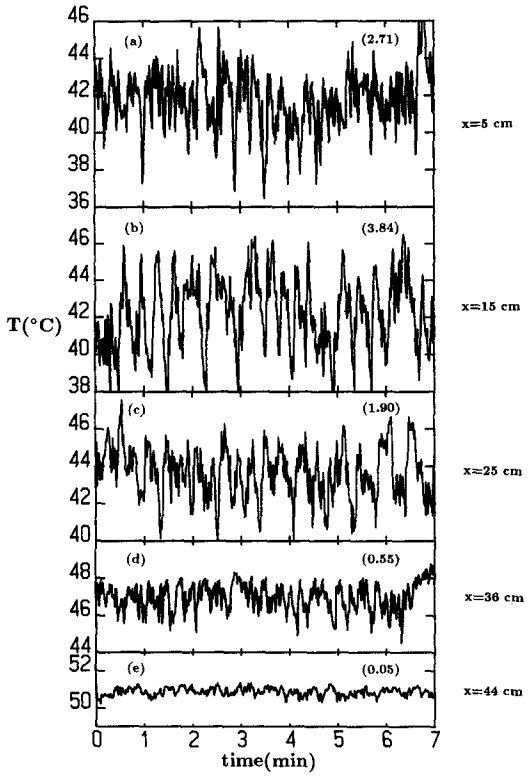

Fig. 6. Temperature fluctuations for opposed convection in a convergent channel with $Gr/Re^2 = 907$ and $Re = 105$ at (a) $x = 5$ cm, (b) $x = 15$ cm, (c) $x = 25$ cm, (d) $x = 36$ cm and (e) $x = 44$ cm.

effect is so large that the temperature fluctuations near the exit for $Gr/Re^2 = 907$ and $Re = 105$ are very similar to the ones for $Gr/Re^2 = 10$ and $Re = 1000$.

Though the evidence provided by the present study is quite limited, the lack of upstream propagation of the influence of flow reversal, as noted in comments associated with Fig. 5, would seem to lend credence to theoretical results obtained using parabolic equations in these flow situations; see, for example, Aung and Worku [40].

Forced convection heat transfer

The pure force convection experiments are performed in a horizontal channel and the results are used for comparison with the mixed convection data. In this case, the top wall is heated and maintained horizontal, while the bottom wall is insulated and is parallel or convergent. It has been shown [26] that for the parallel-plate channel when the Nusselt number is divided by $Re^{0.4}$, the result is independent of the Reynolds number. Therefore, the results for Nusselt number divided by $Re^{0.4}$ are shown in Fig. 7. The figure shows that the normalized Nusselt number which is for the parallel-plate channel for Reynolds number in the range from 500 to 4000 collapses into a single line and the results are slightly higher than the theoretical results of Naito [35]. Note that the prediction of Naito is obtained from an approximate

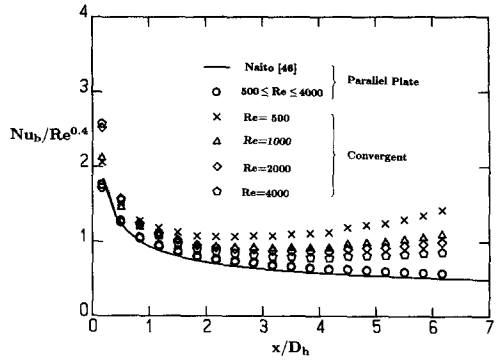

Fig. 7. Comparisons of the normalized Nusselt number for pure forced convection in the convergent and the parallel-plate channel.

solution, which is found to be lower than the exact solution of Heaton *et al.* [36] by 5–7% [37]. Therefore, Naito's predictions are expected to be on the low side. The Nusselt number distribution in the convergent channel is similar to that for turbulent flow in a convergent channel [8]. The Nusselt numbers decrease first owing to the boundary layer growth, reach a minimum and increase thereafter toward the downstream. The increase of the Nusselt number in the downstream region is due to the rapid acceleration of flow. Since the normalized Nusselt number at a lower Reynolds number is larger than that at a higher Reynolds number, the acceleration of flow at a lower Reynolds number is more effective for enhancing the heat transfer. However, the Nusselt number defined above is based on the bulk mean temperature. When the Nusselt number is defined based on the air temperature at the inlet, all the normalized Nusselt numbers for the convergent channel collapse into a single line. An attempt is made to correlate the normalized Nusselt numbers for both the parallel-plate and the convergent channel. The dimensionless parameters selected are x/D_h and A/A_i, where A is the cross section area of the channel perpendicular to the heated plate, and A_i is the cross section area at the inlet of the channel. The ratio A/A_i accounts for the variation of the cross section of the convergent channel. The correlation is found to be:

$$Nu_0/Re^{0.4} = 0.987(x/D_h)^{-0.4}(A/A_i)^{-0.5}. \quad (2)$$

One can also select $(x/D_h)/RePr$ and A/A_i as dimensionless parameter, and equation (2) can be rearranged as follows:

$$Nu_0 = 1.1384\left(\frac{x}{D_h}\Big/RePr\right)^{-0.4}(A/A_i)^{-0.5}. \quad (3)$$

Comparison of the heat transfer data with equation (2) is shown in Fig. 8. The standard deviation of the data from the prediction of equation (2) is 2.5.

Mixed convection heat transfer

For mixed convection, the heated plate is maintained vertical while the opposite wall is parallel or

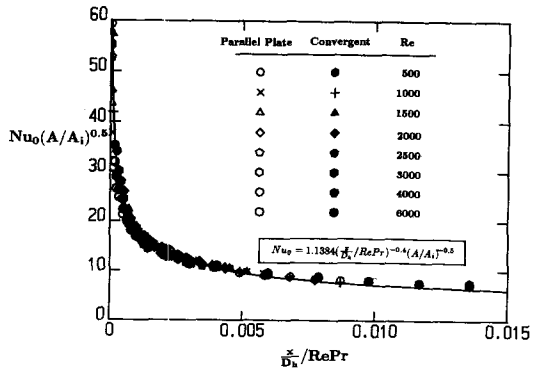

Fig. 8. Correlation of the heat transfer results for pure forced convection in both parallel-plate and convergent channels.

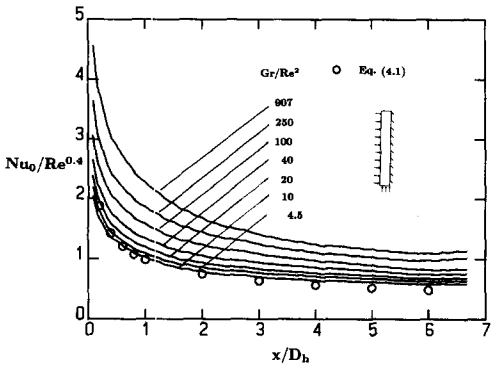

Fig. 9. $Nu/Re^{0.4}$ distributions at different Gr/Re^2 for assisted convection in a parallel-plate channel.

convergent, and the Reynolds numbers range from 105 to 4000. For convenience, the Nusselt number results are normalized by $Re^{0.4}$ and the normalized Nusselt number is found to be independent of Reynolds number. This is true for both parallel-plate and convergent channel. The normalized Nusselt number distributions at different buoyancy parameters for the parallel-plate channel are shown in Fig. 9 and those for the convergent channel are shown in Fig. 10. Both results indicate that the Nusselt number increases with increasing buoyancy parameter except in the region near the exit of the convergent channel. Near the exit region, the flow accelerates so rapidly that the transport process is dominated by forced convection. Therefore, the buoyancy parameter does not have a significant effect on the heat transfer. The normalized Nusselt numbers near the exit at different Gr/Re^2 tend to coalesce and approach the data of pure forced convection.

For assisted convection, the reversed flow occurs along the insulated wall outside the buoyant heated flow for both parallel-plate [27] and convergent channel. It has been shown [27] that for parallel-plate channel the reversed flow has no significant effect either on the temperature distribution inside the buoyant heated flow or the heat transfer along the heated wall. This is also true for the convergent channel. However, the reversed flow in the parallel-plate channel may become unstable, due to mixing with the buoyant heated flow, and transition to turbulent convection occurs which can significantly enhance the heat transfer, especially at the downstream region. For the convergent channel, transition to turbulent flow is not observed, and the reversed flow which appears as a recirculation cell along the insulated wall is very stable and does not have a significant effect on the heat transfer for the experimental range covered.

For assisted convection in parallel-plate channel, the normalized Nusselt number increases in proportion to the buoyancy parameter, as shown in Fig. 9. It appears that the normalized Nusselt number can be correlated in terms of the buoyancy parameter. In addition, one needs also to select a dimensionless distance to account for the local variation of the Nusselt number. The correlation is very successful and the result is written as follows:

$$Nu_0/Re^{0.4} = 0.9232(x/D_h)^{-0.3306} \times [1+0.086(Gr/Re^2)^{0.42}] \quad (4)$$

for $0 \leqslant Gr/Re^2 \leqslant 907$ and $105 \leqslant Re \leqslant 2000$ with a standard deviation of 0.4. The correlation above has included the heat transfer data of pure forced convection. Comparison of the heat transfer data with the prediction of equation (4) is shown in Fig. 11.

For opposed convection in both parallel-plate and

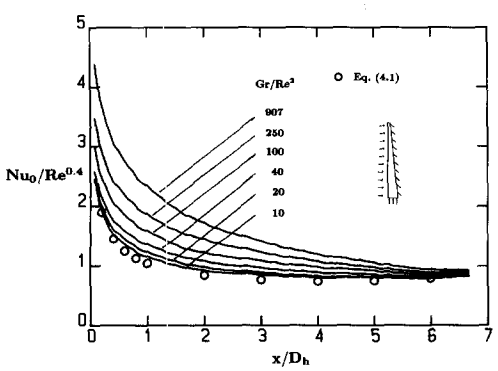

Fig. 10. $Nu/Re^{0.4}$ distributions at different Gr/Re^2 for assisted convection in a convergent channel.

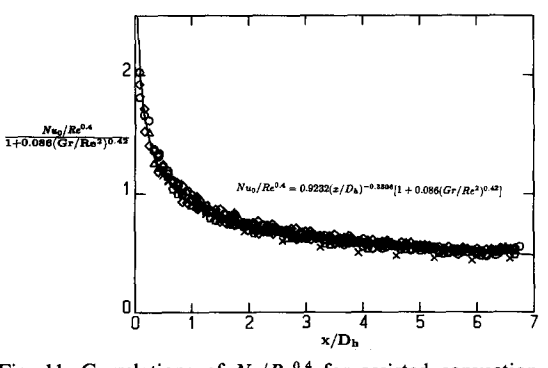

Fig. 11. Correlations of $Nu/Re^{0.4}$ for assisted convection in the parallel-plate channel for $Gr/Re^2 \leqslant 907$ and $105 \leqslant Re \leqslant 2000$.

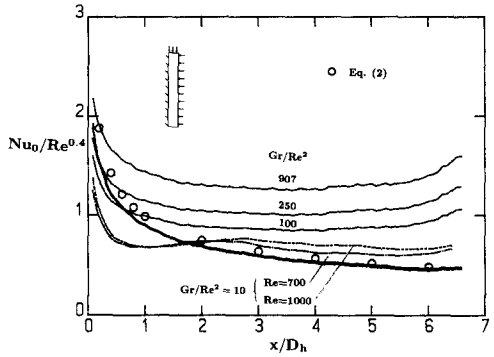

Fig. 12. $Nu/Re^{0.4}$ distributions at different Gr/Re^2 for opposed convection in a parallel-plate channel. The dashed line is for the case of $Gr/Re^2 = 20$ and $Re = 700$.

convergent channel, the Nusselt number can be normalized by $Re^{0.4}$ for $Gr/Re^2 \leqslant 2.5$ or $Gr/Re^2 \geqslant 100$. These are the regimes where either pure forced or natural convection is dominant inside the channel. For $2.5 < Gr/Re^2 < 100$, the normalized Nusselt numbers at different Reynolds number cannot be collapsed into a single line. In this range of buoyancy parameters, the transport processes inside the channel for both free and forced convection are of the same order. The reversed flow can cause a local minimum in the Nusselt number. The increases of the Reynolds number can push the reversed flow downstream which then moves the minimum in the Nusselt number downstream. This leads to the deviation of the normalized Nusselt numbers at different Reynolds number but with the same buoyancy parameter. Although the reversed flow, as discussed previously, is unstable and the separation point moves up and down along the heated wall, the Nusselt number can reach a long-time steady distribution during the experiments. Typical normalized Nusselt number distributions for the buoyancy parameter in this range are plotted as dashed lines as shown in Figs. 12 and 13. The local minimum in the Nusselt number is related to the long-time mean of the separation point of the reversed flow as described in [26].

For buoyancy parameter less than 2.5, the Nusselt number results approach the correlation for pure forced convection, as shown in Figs. 12 and 13. The decrease of the Nusselt number with increasing buoyancy parameter is attributed to the opposed buoyant flow, which retards the velocity near the heated wall and reduces the heat transfer as predicted by Ingham *et al.* [38]. For $Gr/Re^2 \geqslant 100$, the reversed flow is highly unstable and a transition to turbulent convection can occur. This can significantly enhance the heat transfer. The minimum in the Nusselt number, which at current flow condition is not related to the separation point of the reversed flow, could hardly be observed, especially for the convergent channel. In the downstream region, the increase of the Nusselt number as the flow moves downstream is attributed to transition to turbulence, as discussed by Gau *et al.* [26, 27]. In the convergent channel, however, the increase of the Nusselt number is not so significant due to the suppression of turbulence by the accelerated flow.

Figure 14 shows the variation of $\overline{Nu}/Re^{0.4}$ with Gr/Re^2 in the convergent channel. The theoretical results of pure forced convection [36] and the numerical results of pure natural convection in a vertical parallel-plate duct [39] are also plotted for comparisons. The Nusselt number results for pure forced convection in the convergent channel is also presented, and are 20% higher than those for parallel-plate channel due to the rapid acceleration of the flow. For both assisted and opposed convection, the experimental data approach the pure forced convection results for small Gr/Re^2. For opposed convection, however, the average Nusselt number decreases with increasing Gr/Re^2 for small Gr/Re^2 and increases with Gr/Re^2 for large Gr/Re^2. For $Gr/Re^2 \geqslant 100$, when natural convection is dominant, the average Nusselt numbers for both assisted and opposed convection approach each other and the data are very close to those for free convection in the parallel-plate channel. However, the local variation of the Nusselt numbers for both assisted and opposed convection are significantly different, as indicated in the previous section.

The parameter $\overline{Nu}/Re^{0.4}$ for the convergent channel

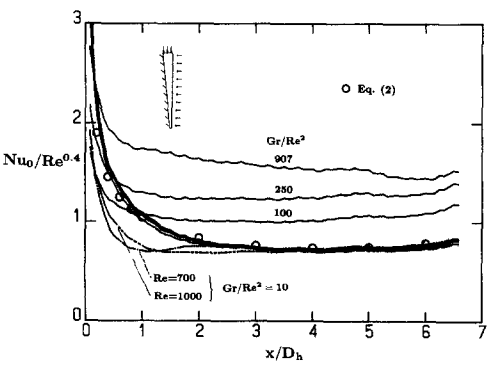

Fig. 13. $Nu/Re^{0.4}$ distributions at different Gr/Re^2 for opposed convection in a convergent channel. The dashed line is for the case of $Gr/Re^2 = 20$ and $Re = 700$.

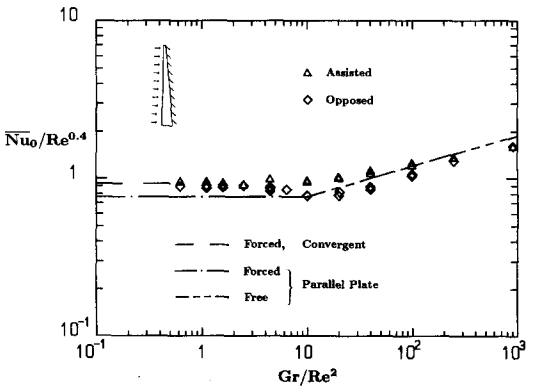

Fig. 14. Variations of $\overline{Nu}/Re^{0.4}$ with Gr/Re^2 for assisted and opposed convection in a convergent channel.

is correlated in terms of Gr/Re^2, and the results are written as follows.

For assisted convection and $Gr/Re^2 \leqslant 907$,

$$100\log(\overline{Nu}/Re^{0.4}) = -3.8+0.4124\log(Gr/Re^2) + 2.6234[\log(Gr/Re^2)]^2 \quad (5)$$

with a standard deviation of 0.011.

For opposed convection and $Gr/Re^2 \leqslant 10$, which is the regime where Nu decreases with increasing Gr/Re^2,

$$100\log(\overline{Nu}/Re^{0.4}) = -4.52+1.314\log(Gr/Re^2) - 3.396[\log(Gr/Re^2)]^2 - 4.279[\log(Gr/Re^2)]^3 \quad (6)$$

with a standard deviation of 0.007.

For opposed convection and $10 \leqslant Gr/Re^2 \leqslant 907$,

$$100\log(\overline{Nu}/Re^{0.4}) = -17.03+9.834\log(Gr/Re^2) + 4.081[\log(Gr/Re^2)]^2 \quad (7)$$

with a standard deviation of 0.014.

CONCLUSIONS

Both forced and mixed convection flow and heat transfer in the convergent channel have been studied experimentally. Reversed flow is found for both assisted and opposed convection. However, flow reversal occurs only in the upstream reaches of the channel but not in the downstream region where rapid acceleration of flow makes forced convection the dominant transport process. The region where the reversed flow traverses extends gradually with increasing buoyancy parameter. For assisted convection, the reversed flow is very steady and appears as a circulation cell along the insulated wall and does not have a significant effect on the heat transfer. For opposed convection, however, due to the counter motion with the mainstream, the reversed flow is unstable and may lead to generation of vortices and transition to turbulent convection. This can significantly enhance the heat transfer. However, the temperature fluctuation measurements indicate that the rapid acceleration of the flow in the downstream can suppress the turbulence intensity and eventually reduce the heat transfer.

Pure forced convection heat transfer in both the parallel-plate and the convergent channel has been measured and correlated. For assisted and opposed convection, both the local and the average Nusselt numbers when divided by $Re^{0.4}$ are found experimentally to be a function only of the buoyancy parameter. However, this is not true for the local Nusselt number in opposed convection within $2.5 < Gr/Re^2 < 100$. For assisted convection, the buoyancy parameter does not have a significant effect on the Nusselt number in the region near the exit, due to the rapid acceleration of flow causing the transport process to be dominated by forced convection. For opposed convection, the increase of the Nusselt number with the buoyancy parameter is attributed to the occurrence of the reversed flow, which has a strong interaction and mixing with the mainstream leading to enhanced heat transfer. Correlations of the average Nusselt number in terms of the buoyancy parameter are also obtained.

Acknowledgement—This research was sponsored by the National Science Council of Taiwan under contract No. NSC 80-0401-E006-38.

REFERENCES

1. H. Schlichting, *Boundary Layer Theory* (4th Edn), p. 107. McGraw-Hill, New York (1960).
2. B. L. Reeves and C. J. Kippenhan, On a particular class on similar solutions of the equations of motion and energy of a viscous fluid, *J. Aerospace Sci.* **29**, 38–47 (1962).
3. K. Millsaps and K. Pohlhausen, Thermal distributions in Jeffery–Hamel flows between nonparallel plane walls, *J. Aeronaut. Sci.* **20**, 187–196 (1953).
4. E. M. Sparrow and J. B. Starr, Heat transfer to laminar flow in tapered passages, *ASME. J. Appl. Mech.* **32**, 684–689 (1965).
5. Y. Shiina, Heat transfer in a tapered passage, *Int. J. Heat Fluid Flow* **8**, 64–71 (1987).
6. J. Dey and G. Nath, Boundary-layer convective heat transfer in a convergent channel, *Lett. Heat Mass Transfer* **8**, 371–377 (1981).
7. J. W. Yang and G. M. Price, Laminar flow development and heat transfer in convergent plane-walled channels, *Appl. Sci. Res.* **25**, 361–371 (1972).
8. J. W. Yang and N. Liao, An experimental study of turbulent heat transfer in converging rectangular ducts, *ASME J. Heat Transfer* **95**, 453–457 (1973).
9. C. C. Su and H. Lin, Forced convection in convergent and divergent ducts of rectangular cross section, *Numer. Heat Transfer* A **20**, 445–458 (1991).
10. C. C. Su and H. Lin, Forced convection in the entrance region of convergent and divergent ducts of rectangular cross section, *J. CSME* **12**(3), 314–319 (1991).
11. K. Komori, A. Iguchi and R. Izumi, Characteristics of turbulent flow in divergent channels of rectangular cross section, *Int. Chem. Engng* **25**, 97–104 (1985).
12. T. Kajiuchi, N. Shiragami and I. Miyagawa, Pressure drop in divergent flow through a tapered tube, *Int. Chem. Engng* **26**, 499–505 (1986).
13. E. M. Sparrow, R. Ruiz and L. F. A. Azevedo, Experimental and numerical investigation of natural convection in convergent vertical channels, *Int. J. Heat Mass Transfer* **31**, 907–915 (1988).
14. E. M. Sparrow and R. Ruiz, Experiments on natural convection in divergent vertical channels and correlation of divergent, convergent and parallel-channel Nusselt numbers, *Int. J. Heat Mass Transfer* **31**, 2197–2205 (1988).
15. T. J. Hanratty, E. M. Rosen and R. L. Kabel, Effect of heat transfer on flow field at low Reynolds numbers in vertical tubes, *Ind. Engng Chem.* **50**, 815–820 (1958).
16. B. R. Morton, Laminar convection in uniformly heated vertical pipes, *J. Fluid Mech.* **8**, 227–240 (1960).
17. D. Maitra and K. Subba Raju, Combined forced and free convection laminar heat transfer in a vertical annulus, *ASME J. Heat Transfer* **97**, 135–137 (1975).
18. J. H. Kim, Analysis of laminar mixed convection in vertical tube annulus with upward flow. In *Fundamentals of Forced and Mixed Convection*, ASME HTD-Vol.42, pp. 91–98 (1985).
19. W. Aung and G. Worku, Theory of fully developed,

combined convection including flow reversal, *ASME J. Heat Transfer* **108,** 485–488 (1986).
20. K. A. Yih, Experimental and numerical study of mixed convection flow and heat transfer in vertical channels, Ph.D. Thesis, Institute of Aeronautics and Astronautics, NCKU, Taiwan, R.O.C., April (1992).
21. W. Aung, Mixed convection in internal flow. In *Handbook of Single-Phase Convective Heat Transfer* (Edited by S. Kakac, R. K. Shah and W. Aung), Chap. 15. Wiley, New York (1987).
22. J. D. Jackson, M. A. Cotton, and B. P. Axcell, Studies of mixed convection in vertical tubes, *Int. J. Heat Fluid Flow* **10,** 2–15 (1989).
23. R. A. Wirtz and P. McKinley, Buoyancy effects on downward laminar convection between parallel-plates. In *Fundamentals of Forced and Mixed Convection*, ASME HTD-Vol. 42, pp. 105–112 (1985).
24. R. A. Wirtz and T. Hamadah, Transitional Reynolds number convection in a vertical channel with opposing buoyancy effects, *Proc. ASME–JSME Thermal Engng Joint Conf.*, Vol. 1, pp. 443–448 (1987).
25. B. J. Baek, D. A. Palaski, B. F. Asrmaly and T. S. Chen, Mixed convection in an asymmetrically heated vertical parallel-plate duct flow, *Proceedings of the 9th International Heat Transfer Conference*, Vol. 2, pp. 369–374 (1990).
26. C. Gau, K. A. Yih and W. Aung, Measurements of heat transfer and flow structure in heated vertical channels, *AIAA J. Thermophys. Heat Transfer* **6,** 707–712 (1992).
27. C. Gau, K. A. Yih and W. Aung, Reversed flow structure and heat transfer measurements for buoyancy-assisted convection a heated ducts, *ASME J. Heat Transfer* **114,** 928–935 (1992).
28. B. W. Webb and D. P. Hill, High Rayleigh number laminar natural convection in an asymmetrically heated vertical channel, *ASME J. Heat Transfer* **111,** 649–656 (1989).
29. N. Fukamachi, Y. Ohya and Y. Nakamura, An improvement of smoke-wire method of flow visualization, *Fluid Dyn. Res.* **169,** 23–29 (1991).
30. T. L. Chen and J. J. Miau, The making and application for hot-film calibration, *Proceedings of the 4th National Conference on Mechanical Engineering*, pp. 147–152. CSME (1987).
31. S. J. Kline and F. A. McClintock, Describing uncertainties in single-sample experiments, *Mech. Engng* **75,** 3–12 (1953).
32. C. Gau, K. A. Yih and W. Aung, Numerical and analytical study of reversed flow and heat transfer in a heated vertical duct. In *Mixed Convection Heat Transfer*, ASME HTD-Vol. 247, 9–19 (1993).
33. P. M. Moretti and W. M. Kays, Heat transfer to a turbulent boundary layer with varying free-stream velocity and varying surface temperature, *Int. J. Heat Mass Transfer* **8,** 1187–1202 (1965).
34. H. Tanaka, H. Kawamura, A. Tateno and S. Hatamiya, Effect of laminarization and retransition on heat transfer for low Reynolds number flow through a converging to constant area duct, *ASME J. Heat Transfer* **104,** 363–371 (1982).
35. E. Naito, Laminar heat transfer in the entrance region between parallel-plates—the case of uniform heat flux, *Heat Transfer-Jap. Res.* **4**(2), 63–74 (1975).
36. H. S. Heaton, W. C. Reynolds and W. M. Kays, Heat transfer in annular passages. Simultaneous development of velocity and temperature fields in laminar flow, *Int. J. Heat Mass Transfer* **7,** 763–781 (1964).
37. R. K. Shah and A. L. London, Laminar flow forced convection in ducts. In *Advances in Heat Transfer*, Supplement 1. Academic Press, London (1978).
38. D. B. Ingham, D. Keen and P. J. Heggs, Two dimensional combined convection in vertical parallel plate ducts, including situations of flow reversal, *Int. J. Numer. Meth. Engng* **26,** 1645–1664 (1988).
39. W. M. Yan and T. F. Lin, Natural convection heat transfer in vertical open channel flows with discrete heating, *Proceedings of the 3rd National Conference on Mechanical Engineering*, Vol. 1, No. 2, pp. 157–167. CSME (1986).
40. W. Aung, and G. Worku, Developing flow and flow reversal in vertical channel with asymmetric wall temperatures, *ASME J. Heat Transfer* **108,** 299–304 (1986).